# Experimental Investigation and Comparison of Approaches for Correcting Acceleration Phases in Motor Torque Signal of Electromechanical Axes

Chris Schöberlein[a], André Sewohl[b], Holger Schlegel and Martin Dix[c]
*Institute for Machine Tools and Production Processes, Chemnitz University of Technology, Reichenhainer Str. 70, 09126 Chemnitz, Germany*

Keywords: Electromechanical Axis, Industry 4.0, System Identification, Acceleration Correction.

Abstract: Electromechanical axes are an essential factor for productivity in almost all common production systems. In context of Industry 4.0, using integrated sensors for machine monitoring is gaining importance in recent years. In addition to the well-known condition monitoring of mechanical components, the internal control loop signals are capable to estimate external load forces, e.g. caused by production process. However, this requires the separation of all motor-related signal components from the external loads. The paper contributes to this topic by comparing multiple approaches for detecting acceleration and braking phases during conventional axis movements and examines the subsequent correction of associated components in motor torque signal. All approaches exclusively use signals available in the drive and control system. Extensive experiments on a single-axis rotary test rig show general suitability as well as limitations of the presented methods.

## 1 INTRODUCTION

Motion generation in production machines is mainly realized with the aid of electromechanical axes. They are used as auxiliary drives to generate feed motions and hence, in case of metal-cutting machine tools, maintain chip removal as well as all other necessary positioning, infeed or tool change movements. Furthermore, they are deployed as main drive of servo screw presses. Their application area also covers a wide range of other production systems, e.g. for conveying, positioning and synchronization applications, in printing and textile machines as well as in packaging, filling and assembly systems.

Utilization of electromechanical axis for machine monitoring is increasingly coming into focus, especially in connection with Industry 4.0. Besides the condition monitoring of the integrated control loops (Quellmalz et. al., 2016) or mechanical axis components (Schöberlein et. al., 2022), an estimation of externally acting load forces and torques is one major demand. Particular applications are the estimation of process forces during milling, drilling, turning or grinding (cf. Kaever 2004, Aslan and Altintas, 2018, Aslan, 2019, Yamato et. al., 2019), chatter suppression in milling and drilling (cf. Yoneka et. al., 2012, Sugiyama et. al., 2017, Yamato et. al., 2021) or the detection of collisions (cf. Rehse, 1999, Rudolf, 2014) in the working frame of machine tools. According to Eq. (1), the sum of all load torques $T_l$ is measurable as reaction in motor torque signal $T_m$.

$$T_m=T_a+T_l \tag{1}$$

According to Eq. (2), the load torque can be further devided into several parts. Besides an external load torque $T_{l,e}$, it consists of friction and gravity related torques ( $T_f$ and $T_g$ ) as well as other disturbance torques $T_{l,d}$ (e.g. cogging torques).

$$T_l=T_{l,e}+T_f+T_g+T_{l,d} \tag{2}$$

Hence, an estimation of external load torques requires the knowledge of all other torque components. While an identification of gravity and

[a] https://orcid.org/0009-0006-3603-5012
[b] https://orcid.org/0000-0003-2031-6603
[c] https://orcid.org/0000-0002-2344-1656



Schöberlein, C., Sewohl, A., Schlegel, H. and Dix, M.
Experimental Investigation and Comparison of Approaches for Correcting Acceleration Phases in Motor Torque Signal of Electromechanical Axes.
DOI: 10.5220/0012160600003543
In *Proceedings of the 20th International Conference on Informatics in Control, Automation and Robotics (ICINCO 2023) - Volume 1*, pages 140-151
ISBN: 978-989-758-670-5; ISSN: 2184-2809

friction induced load torques and the subsequent correction of the measured motor torque was already shown in (Schöberlein et. al., 2022c), an appropriate acceleration correction is still required.

Hence, the aim of this paper is to identify and correct acceleration phases in motor torque signal during conventional axis movements. In chapter 2, different approaches are researched and extended or newly developed. A distinction is made between methods that are based on actual or command position signal, respectively. One main contribution to the topic is made by chapter 3, in which all approaches are investigated by extensive experiments carried out on a modular drive test rig. This is followed by a discussion of results and subsequent derivation of recommendations for specific applications. The paper concludes with a summary and an outlook for further research.

# 2 METHODOLOGY

## 2.1 Acceleration Correction Based on Actual Position Values

Acceleration torque $T_a$ is calculated as product of angular acceleration $\ddot{\varphi}_m$ and total moment of inertia $J_{tot}$ reduced to motor shaft.

$$T_a = \ddot{\varphi}_m \cdot J_{tot} \tag{3}$$

Since angular acceleration is usually not available as measurable parameter in the controller, it is calculated from the angular position $\varphi_m$ by twofold discrete differentiation. The resulting acceleration torque, hereafter referred to as $\hat{T}^m_{a,1}$ (motor-side position measurement) or $\hat{T}^l_{a,i1}$ (load-side position measurement), is applied, for example, in the works of (Aslan and Altintas, 2018) and (Aslan, 2019) as part of an approach for drive-based reconstruction of process forces in five-axis milling. Similar approaches based on different variants of order-reduced disturbance observers were already proposed in several publications (e.g. Isshiki et. al., 2021). One disadvantage is the assumption of a rigid or strongly reduced order mechanical structure and hence required low-pass filtering below the first mechanical natural frequency. It is also mandatory to determine the total moment of inertia based on construction data or using an appropriate identification method (cf. (Hofmann et. al., 2010), (Hellmich et. al., 2011) or (Hipp et. al., 2017)).

In the following, a novel approach based on Eq. (3) is proposed and extended for complex multi-mass mechanics including an automatic parameter identification routine (figure 1). Basic idea is to model the frequency response from motor or load angular velocity to motor torque by linking a rigid single mass system (Eq. (4)) with several partial oscillators (PO) according to Eq. (5) (Schöberlein et. al., 2022b).

$$G_s(s) = \frac{1}{J_{tot} \cdot s} \tag{4}$$

$$G_{PO}(s) = \frac{a \cdot \frac{1}{\omega_f^2} \cdot s^2 + \frac{2d_f}{\omega_f} \cdot s + 1}{\frac{1}{\omega_r^2} \cdot s^2 + \frac{2d_r}{\omega_r} \cdot s + 1} \tag{5}$$

$J_{tot}$ denotes the total moment of inertia, while $\omega_r$ and $\omega_f$ are the resonance and antiresonance frequencies of the partial oscillator with associated damping values $d_r$ and $d_f$. By assigning parameter $a$ with zero or one, the partial oscillator characteristic is adjusted for direct or indirect case, respectively (Schöberlein et. al., 2022b). Multiplying (4) with (5) leads to

$$G_s^{m,l}(s) = \frac{\omega_{m,l}}{T_m} = G_s(s) \cdot \prod_{i=1}^{n} G_{PO,i}(s) \tag{6}$$

$G_s^{m,l}(s)$ represents the transfer function between angular velocity measured on motor ($\omega_m$) or load side ($\omega_l$) and motor torque $T_m$. The number of partial oscillators n depends on the order of the mechanical system or desired modeling depth. Setting $n = 1$ results in the well-known two-mass system. By initially assuming that no internal or external load moments are present ( $T_m = T_a$ ), Eq. (6) can be rearranged as follows

$$T_a^{m,l} = \omega_{m,l} \cdot G_s^{m,l}(s)^{-1} \tag{7}$$

Hence, besides an identification of transfer functions according to (6), their subsequent inversion is also necessary. Furthermore, all models must be transferred into discrete-time representation to enable an implementation on control systems with fixed sample times. For this purpose, a five-step procedure (figure 1) was developed, which has already been successfully applied on a three-axis milling machine (Schöberlein et. al., 2022b).

In a first step, the axis is excited with pseudo-binary noise signal at level of current setpoint filter output while recording actual values for motor torque $T_m$ and angular motor velocity $\omega_m$. If there is an additional load-side encoder, a second transfer function for load-side angular velocity $\omega_l$ can be used. In case of linear axes, the feed rate signal is converted considering the values for gear ratio and spindle pitch.

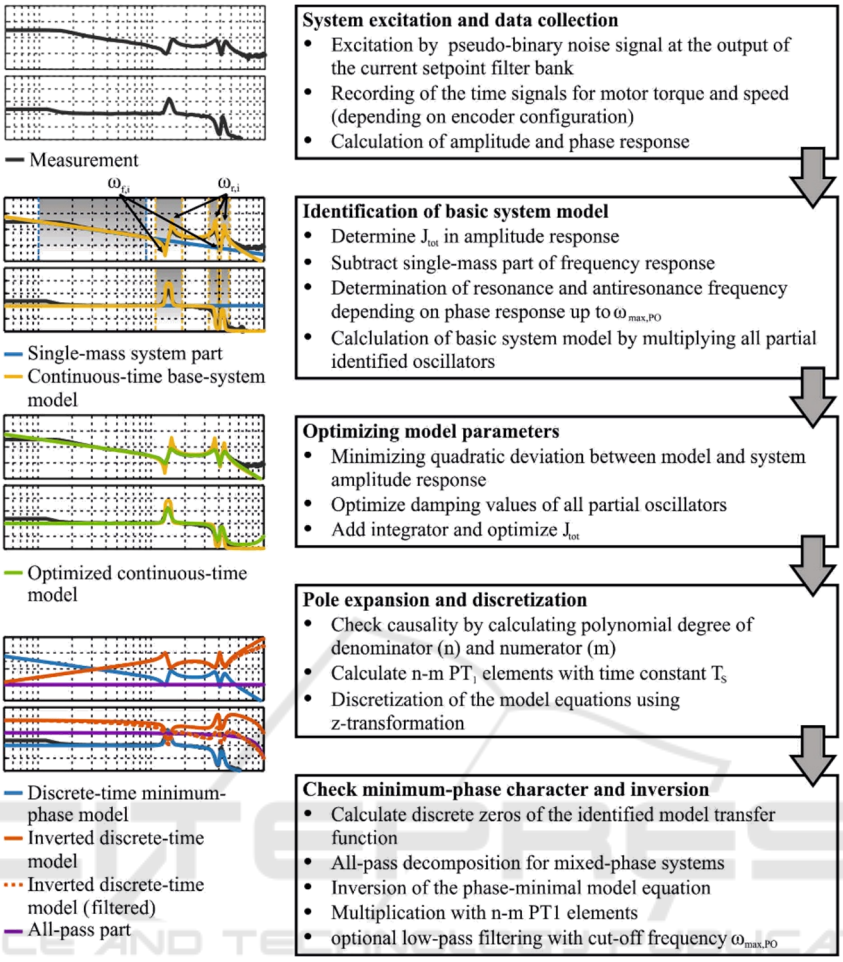


Figure 1: Methodology for identification and discrete inversion of multi-mass systems.

Subsequently, a basic system model is determined. Therefore, a linear model for $J_{tot}$ is approximated in low-frequency range with a slope of -20 dB per decade. By subtracting the linear part, values for resonance and antiresonance frequencies ($\omega_r$ and $\omega_f$) of i partial oscilators according to Eq. 4 are identified. Setting parameter a to zero or one depends on the phase characteristic of the corresponding partial oscillator. The value of a becomes one when the phase angle rotates in positive or negative direction up to a previously defined threshold (e.g. 50 °), remains in a specified frequency band and subsequently performs significant reverse rotation in opposite direction. If, on the other hand, a phase rotation of -180 ° takes place without subsequent reversal, this indicates a partial oscillator with a set to zero. Furthermore, aliasing effects in upper frequency band require the definition of a cutoff frequency $\omega_{max,PO}$ up to which the phase response is searched for partial oscillators (Siemens, 2012).

The exact determination of resonance and antiresonance frequencies is based on subsequent extreme value search in amplitude response in range of the previously detected partial oscillator limits. An extension of the frequency limits by 10 percent ensures a reliable detection. This leads to a general overall transfer function in product form. Damping parameters were assigned with initial values ($d_{f,i} = d_{r,i} = 0.01$) for each partial oscillator (cf. Eq. 5).

Subsequently, the estimation of damping values is carried out by minimizing the squared deviation between measured and modeled frequency response using Nelder-Mead optimizer. Therefore, an optimization function integrated in MATLAB® based on the methodology from (Nelder and Mead, 1965) was used. If the optimizer is also applied to the single-mass model, the estimation accuracy of $J_{tot}$ can be further improved.

In the next step, an inversion and discretization of the estimated model function is required to calculate the acceleration torque from measured rotational

speed. Regardless of the specific transfer function, the polynomial degree of the denominator n is higher than the degree of the numerator m. In case of a direct inversion, this relationship is reversed, which leads to a violation of the causality principle due to the differential character of the resulting transfer function (Schröder, 2007). In this paper, the proposed solution for a stable inverted transfer function is based on an extension by n-m high-frequency poles (Eq. 9 and 10). The time constant is set equal to control sampling time $T_S$.

$$G_s(s)^{-1} = \frac{1}{G_s(s)} \cdot G_{Pol}(s) \tag{8}$$

$$G_{Pol}(s) = \frac{1}{(1+T_S \cdot s)^{n-m}} \tag{9}$$

Furthermore, an implementation on fix sampled computing systems requires a transfer of continuous-time models into discrete-time representation. This is carried out by applying z-transformation and thus rhe mapping of the s-plane to the z-plane according to Eq. (11) with control sampling time $T_S$ (Graf, 2012).

$$z = e^{T_S \cdot s} \tag{10}$$

Eventually, an inversion of the model equations is carried out. Especially in case of load-side and mechanical transfer functions, the resulting models may have non-minimum-phase character. This means that the transfer function shows one or more unstable zeros, which is expressed in pole-zero diagram by their location outside of the unit circle. By inverting the model equation, all zeros become poles and vice versa. Consequently, the inverted transfer function would have the same number of unstable poles, which results in an unstable system itself. In this case, the transfer function is decomposed into one minimum-phase and n all-pass components. Starting point is the general representation of discrete transfer functions in product form according to Eq. 12.

$$G(z) = \frac{\left(\prod_{i=1}^{M_1}(1-z_i z^{-1})\right) \cdot \left(\prod_{i=1}^{M_2}(1-q_i z^{-1})\right)}{\prod_{i=1}^{n}(1-p_i z^{-1})} \tag{11}$$

Parameter $p_i$ denote the poles, whereas $z_i$ are all zeros inside and $q_i$ outside of the unit circle. A decomposition in a minimum-phase part $G_{MP}(z)$ and an allpass part $G_{AP}(z)$ is carried out according to Eq. (13) – Eq. (15) with $q_i^*$ as new stable zeros.

$$G(z) = G_{MP}(z) \cdot G_{AP}(z) \tag{12}$$

$$G_{MP}(z) = \frac{\left(\prod_{i=1}^{M_1}(1-z_i z^{-1})\right) \cdot \left(\prod_{i=1}^{M_2}(q_i^* - z^{-1})\right)}{\prod_{i=1}^{n}(1-p_i z^{-1})} \tag{13}$$

$$G_{AP}(z) = \frac{\left(\prod_{i=1}^{M_2}(1-q_i z^{-1})\right)}{\prod_{i=1}^{n}(q_i^* - z^{-1})} \tag{14}$$

The magnitude response of the minimum-phase model $G_{MP}(z)$ remains unchanged compared to the original system G(z), since the magnitude of the all-pass components $G_{AP}(z)$ is one for all frequencies. On the other hand, the phase response shows a significant drop in upper frequency band. For more details on the procedure see (Schilling and Harris, 2016). For subsequent inversion, only the product of the minimum-phase component and magnitude of the all-pass component is used. Although this results

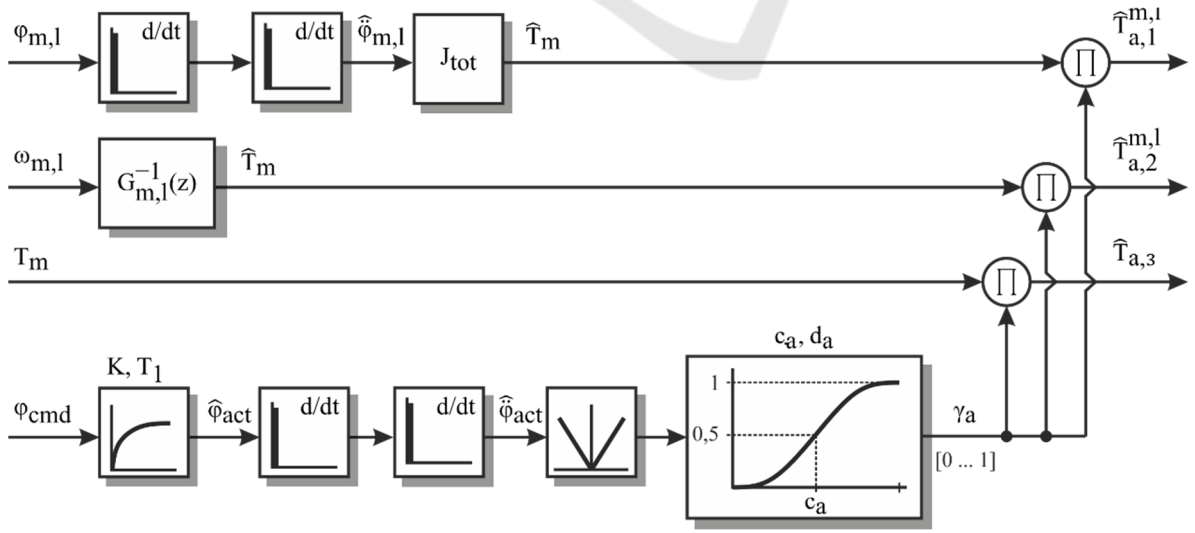


Figure 2: Approaches for estimating and correcting acceleration torque based on actual position values in combination with command-value based weighting.

in a slight phase shift of the inverted transfer function, experiments in chapter 3 show that these are neglectable. Alternative approaches for an inversion of mixed-phase systems based on non-recursive filters or Kalman Filters can be found in (Aslan, 2019).

A fundamental disadvantage of both presented approaches is the possible compensation of unintentional acceleration phases (e.g. reaction to external loads). Consequently, a mechanism that solely detects acceleration phases caused by changes in command values is required. Therefore, a combination of the estimated motor torque $\hat{T}_m$ and a setpoint-based acceleration detection following the approach presented in (Rudolf, 2014) is proposed (figure 2, bottom).

Fundamental idea is to multiply the estimated motor torque $\hat{T}_m$ with an acceleration index $\gamma_a$. Based on thw motor command position $\varphi_{cmd}$, an artificial actual position $\hat{\varphi}_{act}$ is calculated using a $PT_1$ model (first order lag element) with gain K equal to one. Selecting time constant $T_1$ inversely proportional to position control gain factor $K_v$ allows adapting the estimation to the dynamic behaviour of the axis.

$$T_1 = \frac{1}{K_v} \tag{15}$$

After double derivation of $\hat{\varphi}_{act}$, theestimated acceleration value $\hat{\ddot{\varphi}}_{act}$ is weighted by a sigmoidal function. This ensures that the acceleration index $\gamma_a$ only takes values between zero and one. Reliable detection of deceleration movements is granted by calculating the absolute value of $\hat{\ddot{\varphi}}_{act}$. Parameter $c_a$ defines for which acceleration value $\gamma_a$ reaches 0.5. On the other hand, $d_a$ defines the slope at this point (Rudolf, 2014). For the experimental setup used in this paper, assigning $c_a = 0{,}001 \cdot \ddot{\varphi}_{M,max}$ and $d_a = 0{,}0001 \cdot \ddot{\varphi}_{M,max}$ leads to satisfactory results.

In case of a precisely set acceleration detection, it is also possible to use the actual value of $T_m$ directly. In the following, this approach is entitled $\hat{T}_{a,3}$. This variant corresponds to a zero setting of the torque signal in case of detected acceleration.

## 2.2 Acceleration Correction Based on Command Position Values

However, all actual value-based methods have in common that the detection of critical load cases (e.g. due to collision) during acceleration phases is not readily possible. Alternatively, an exclusive utilization of controller-generated setpoint values combined with a more or less detailed model of the drive control loops can be applied. However, due to the complexity of the cascaded control including application-specific feedforward control and setpoint filters, a detailed modelling is not possible with reasonable efford. On the other hand, theoretically developed reduced-order models as described in (Groß et. al., 2006) or (Hofmann et. al., 2010) lead to significantly reduced estimation accuracy.

Following the methodology presented in (Kaever, 2004), which is based on an identification of $PT_t$ models, we propose an alternative approach for command value-based estimation of acceleration torque ($\hat{T}_{a,4}$). Fundamental idea is to estimate the transfer behavior between given setpoint acceleration $\hat{\ddot{\varphi}}_{cmd}$ and resulting actual acceleration $\hat{\ddot{\varphi}}_{act}$ based on a scalable $PT_n$ transfer function using least squares method (figure 3). Acceleration torque $\hat{T}_{a,4}$ is calculated by multiplying the estimated acceleration $\hat{\ddot{\varphi}}_{act}$ with total moment of inertia $J_{tot}$. Values for acceleration and torque limits ($\ddot{\varphi}_{max}$ and $T_{m,max}$) are taken from control or drive data, respectively. By estimating transfer functions of different order and subsequent error measure selection (e.g. integral of abolute error, integral of squared error, absolute distance), the transfer behavior can be automatically adapted to the dynamics of the respective axis. During the experimental investigation, a combination of a $PT_1$ element with time constant $T_1$ for dead-time approximation (cf. Hofmann et. al., 2010) and an oscillatory $PT_2$ element with gain K, damping D, and time constant $T_2$ showed satisfactory results. Applying the Padé approximation based on an all-pass element with selectable order is also feasible for dead time approximation (Brand, 2002).

Identification of model parameters is carried out experimentally by applying a positioning ramp with defined command speed and subsequent estimation via least squares method in MATLAB®. For low velocities with poor signal-to-noise ratio, the identification results benefit from an appropriate low-pass filtering (e.g. moving average) of the measured acceleration signal. Note that changes in speed

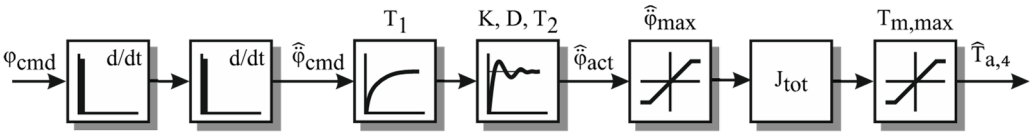


Figure 3: Signal flow chart of acceleration correction with $PT_2$ substitute model ($\hat{T}_{a,4}$).

command also result in minor differences for the identified parameter values. To quantify this effect, a speed-individual parameterization is compared with a fixed setting based on an identification in medium speed band in chapter 3. In contrast to actual-value-based approaches, changes in drive dynamics (e.g. when adjusting parameters of drive control loops) require a further parameter identification.

# 3 RESULTS

## 3.1 Test Setup

Experimental investigation of all presented approaches is carried out on a modular drive test rig with rotational mechanics. Its overall mechanical structure is illustrated in the left part of figure 4. The test rig is equipped with a SIMOTION D445 motion control system and a subordinate SINAMICS drive system. It provides all required basic functions (noise generator, signal recording) for determining transfer functions and signal measurement. The mechanical system consists of a position-controlled servomotor for converting motion setpoints (1) specified by the control system and an identical synchronous motor on load side for impressing dynamic load torques (9), measurable with an additional torque sensor (8). A toothed belt drive (2) with transmission ratio $i_G = 1$ connects drive and load side. Besides the motor-integrated position sensors (2048 increments), another incremental rotary encoder (3) with 4096 increments enables modeling of partial transfer functions. All position sensors are incremental sine-cosine encoders. Based on the right part of figure 4, the theoretically calculated total moment of inertia of the experimental setup is $J_{tot} = 0{,}0055763\ kg{\cdot}m^2$. Toothed belt and bearings are assumed to be massless.

All approaches are evaluated in terms of their estimation quality by investigating several positioning sequences with varying speed specification. The nomenclature for the acceleration torque estimation is defined as follows:

- Variant $V_1$: weighted product of total moment of inertia and actual acceleration according to equation (1) ($\hat{T}_{a,1}^{m,l}$),
- Variant $V_2$: inverse filtering of actual angular velocity and weighting via sigmoidal function ($\hat{T}_{a,2}^{m,l}$),
- Variant $V_3$: weighting of actual motor torque value ($\hat{T}_{a,3}$),
- Variante $V_{4a,b}$: calculation based on command position with identified $PT_2$ model ($\hat{T}_{a,4}$).

Additionally, the influence of the measurement system for calculating angular acceleration or angular velocity is investigated. Besides the internal motor sensor, the external encoder with higher resolution is used. In case of $V_1$ and $V_4$, total moment of inertia is set to theoretically determined value $J_{tot} = 0{,}0055763\ kg{\cdot}m^2$. Acceleration and torque limits for variant $V_4$ are set equal to control internal values. Additionally, the parameters for the $PT_2$ model are either calculated individually for each motion profile ($V_{4a}$) or averaged for the whole test series and ($V_{4b}$). The transfer functions for inverse filtering according to variant $V_2$ result from identified parameters (cf. Table 2).

The selected positioning profiles in table 1 distinguish whether acceleration torque result from

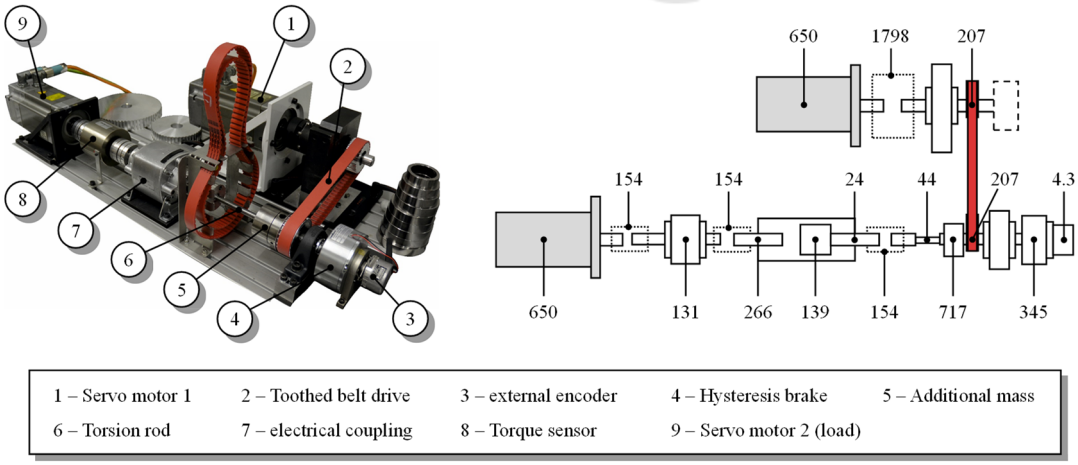


Figure 4: Structure of drive test rig (left) and moments of inertia (all data in kg·mm², taken from data sheets).

standstill or from a given speed setpoint. Furthermore, the direction of movement as well as acceleration and deceleration phases are varied. All drive controller parameters are set according to an automatic commissioning routine and remain unchanged during the experiments. Only acceleration and jerk limits are increased by a factor of ten compared to the preset value. This deliberately dynamically chosen parameterization serves to show limits of the individual approaches. All combinations and the associated parameter specifications are listed in table 1.

Table 1: Parameters for rotary axis test stand.

| Parameter | Value |
|---|---|
| Amplitude | |
| $A_1$ | ±10 $min^{-1}$ |
| $A_2$ | ±50 $min^{-1}$ |
| $A_3$ | ±100 $min^{-1}$ |
| $A_4$ | ±200 $min^{-1}$ |
| $A_5$ | ±400 $min^{-1}$ |
| Offset | |
| $O_1$ (Acceleration) | 0 $min^{-1}$ |
| $O_2$ (Acceleration) | $0.5 \cdot A_i$ |
| $O_1$ (Braking) | $1 \cdot A_i$ |
| $O_2$ (Braking) | $2 \cdot A_i$ |
| Acceleration and jerk limit | |
| $\ddot{\varphi}_{max,1}$ | 100 $s^{-2}$ |
| $\ddot{\varphi}_{max,2}$ | 1000 $s^{-2}$ |
| $\dddot{\varphi}_{max,1}$ | 2000 $s^{-3}$ |
| $\dddot{\varphi}_{max,2}$ | 20000 $s^{-3}$ |

## 3.2 Parameter Identification and Setting

Table 2 lists all identified model parameters for variant $V_2$ according to the described procedure in figure 1. In addition, figure 5 shows the Bode plot of measured (gray), discrete-time (blue) and inverted (orange) frequency responses for motor (left) and external encoder (right). Regardless of encoder configuration, both identified models show high agreement with the measurement, especially in amplitude response.

However, due to discretization of continous-time models, a phase drop in upper frequency band arises. In addition, the load side transfer function $G_s^l(z)$ has one unstable zero. However, by subtracting the all-pass part (purple) according to Eq. (13) to Eq. (15) and subsequent inversion of remaining minimum-phase part (green dashed), a stable inverse transfer function is obtained. Considering the compensated signal (yellow), it becomes clear that the inverse transfer function for both encoder configurations leads to appropriate results over a wide frequency band. Nevertheless, a significant phase drop is noticeable depending on the transfer function.

Table 2: Set and identified Parameters depending on encoder used for actual vaue-based acceleration torque correction.

| Parameter | $G_s^m(z)$ | $G_s^l(z)$ |
|---|---|---|
| Setting Parameters | | |
| $\omega_{min}$ in Hz | 10 | 30 |
| $\omega_{max,J}$ in Hz | 80 | 60 |
| $\omega_{max,P0}$ in Hz | 530 | 600 |
| $\varphi_{min,m}$ in ° | 50 | 50 |
| $\varphi_{min,l}$ in ° | 120 | 120 |
| Identified Parameters | | |
| $J_{tot}$ in kg·$m^2$ | 0.005357 | 0.004834 |
| $\omega_{f,1}$ in Hz | 116.37 | 134.55 |
| $d_{f,1}$ | 0.05 | 0.04 |
| $\omega_{r,1}$ in Hz | 146.47 | 149.11 |
| $d_{r,1}$ | 0.03 | 0.04 |
| $\omega_{f,2}$ in Hz | 304.05 | 32.41 |
| $d_{f,2}$ | 0.05 | 0.30 |
| $\omega_{r,2}$ in Hz | 364.47 | 372.41 |
| $d_{r,2}$ | 0.06 | 0.05 |
| $\omega_{f,3}$ in Hz | 425.38 | 407.12 |
| $d_{f,3}$ | 0.01 | 0.02 |
| $\omega_{r,3}$ in Hz | 432.94 | 448.22 |
| $d_{r,3}$ | 0.05 | 0.05 |

## 3.3 Experimental Investigation and Comparison

In the following, all discussed approaches are investigated by applying the positioning profiles listed in table 1. Note that friction torque was subtracted beforehand using a static model approach (cf. Schöberlein et. al., 2022c). Hence, smaller deviations naturally occur in the resulting motor torque. However, since this applies to all approaches to the same extent, it does not affect the comparison results. Figure 6 depicts the results for estimation and correction in case of one exemplary position profile ($A_1$-$O_1$- $\ddot{\varphi}_{max,1}$ - $\dddot{\varphi}_{max,1}$ ). Besides measured motor torque (black), estimated acceleration torques (dashed) and associated deviations for $V_1$ (a), $V_2$ (b), $V_3$ (c) and $V_4$ (d) are shown. In addition, areas with acceleration index $\gamma_a$ greater than zero are highlighted. Note that for variant $V_4$, model parameters were calculated individually for this specific motion profile.

Comparing approaches $V_1$ (blue and orange) and $V_2$ (yellow and green), a significant reduction in

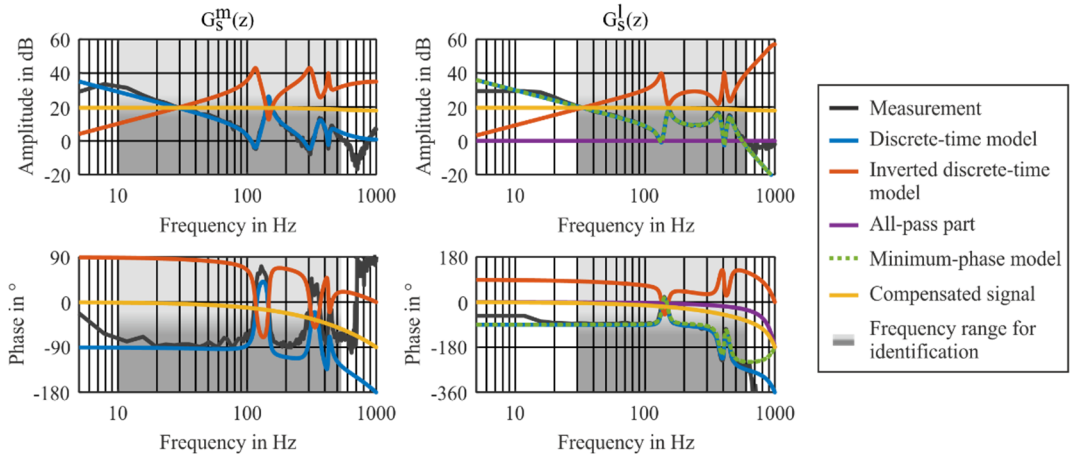


Figure 5: Comparison of measured, discretely modeled and inverted frequency responses for $G_s^m(z)$ (left) and $G_s^l(z)$ (right).

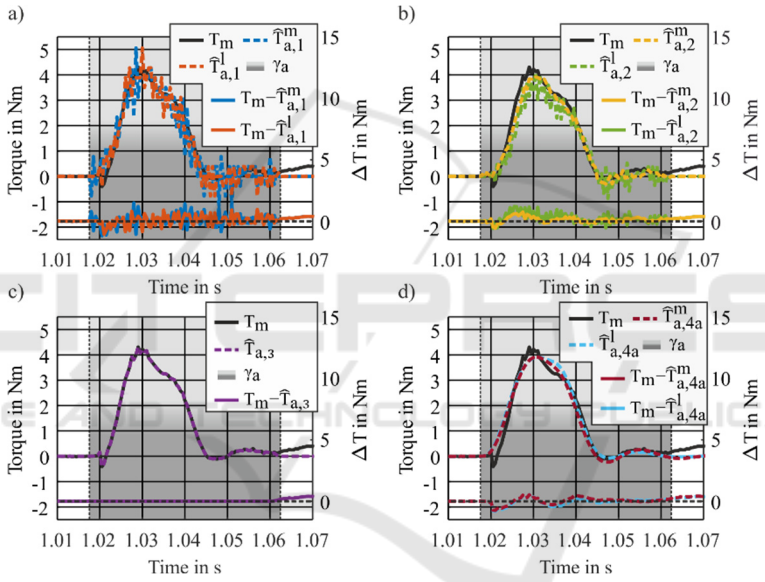


Figure 6: Exemplary signals for measured motor torque and estimated acceleration torque as well as modelling error for approaches $V_1$ (a), $V_2$ (b), $V_3$ (c) and $V_4$ (d).

signal noise in case of the inverse filtering is achieved. Due to lower amplitude gain in upper frequency band, the motor-based approach offers marginal advantages over a load-based model. Furthermore, the underestimated value for total moment of inertia compared to theoretically calculated value leads to recognizable deviations in case of $\hat{T}_{a,2}^l$. As mentioned in chapter 2, an additional frequency response measurement with reduced bandwidth may further increase the model accuracy.

Naturally, ideal correction behavior for the area covered by weighting factor $\gamma_a$ is obtained by approach $V_3$ (purple). The estimation quality of $V_4$ (light blue and red) is comparable to $V_2$ in terms of average deviation, but without any signal noise. Identification of model parameters using load-side acceleration signal (red) results in only minor differences for the estimated acceleration torque.

If one compares the individual approaches based on all motion profiles specified in table 1, the results of the exemplary measurement are confirmed. For clarity, figure 7 only depicts the integral of absolute error $A_{IAE}$ according to Eq. 17 over the weighting area.

$$A_{IAE}=\int_{t_1}^{t_2}\left|T_m(t)-\hat{T}_a(t)\right|\cdot dt \qquad (16)$$

Since the width of the weighting area is not constant for all motion profiles, $A_{IAE}$ is normalized taking into account the number of included sampling

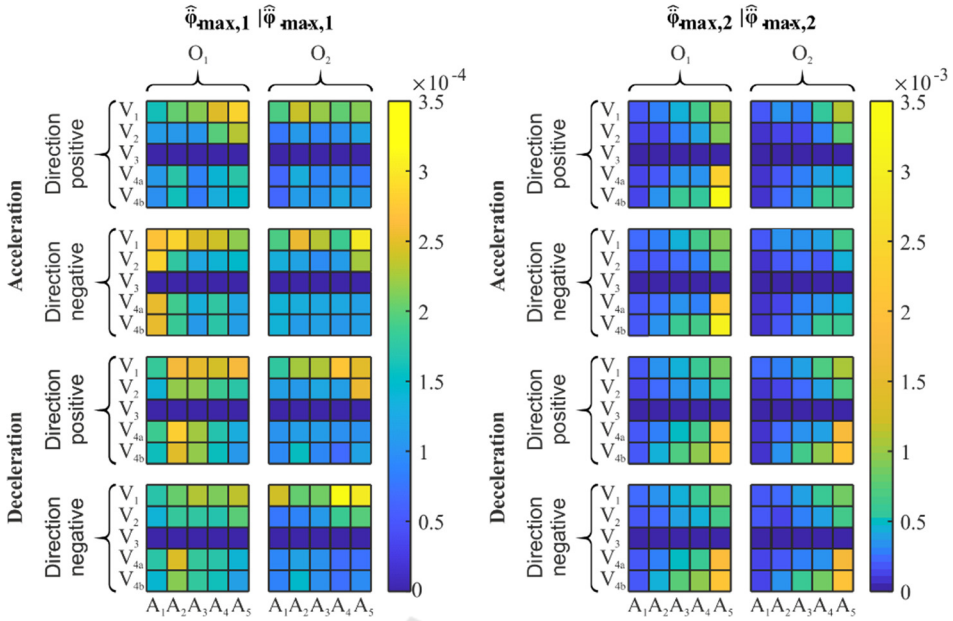


Figure 7: $A_{IAE}$ of acceleration correction approaches for all motion profiles with preset (left) and increased values for acceleration and jerk limitation (right).

points. Due to deviations in friction correction as well as not yet included standstill torque compensation, minor differences in $A_{IAE}$ for acceleration and deceleration may occur for identical approaches. This is particularly noticeable for deceleration movements to standstill. However, these phenomena are not significant for a comparison of the concepts in the respective positioning sequence.

On the other hand, the load-side encoder leads only in exceptional cases to a significant improvement of estimation accuracy. Hence, only results using motor internal encoder are considered in the following. This can also be justified by the fact that not every electromechanical axis is equipped with an additional load-side position sensor. For the command value-based approach, $V_{4a}$ indicates an individual parameter identification for the corresponding motion sequence while $V_{4b}$ determines an overall parametrization.

The left part of figure 7 shows the $A_{IAE}$ for all motion sequences with preset values for acceleration and jerk limits ($\dot{\varphi}_{max,1}$ and $\ddot{\varphi}_{max,1}$). As expected, variant $V_3$ leads to an ideal correction independent of the given motion profile. This is followed by command value-based approaches $V_{4a}$ and $V_{4b}$. A general parameter set of the $PT_2$ model based on mean values over all motion sequences leads to an equivalent or even better correction. Considering actual-value-based approaches $V_1$ and $V_2$, a more complex model of the mechanical system leads to smaller deviations between measured and modeled acceleration torque for all sequences. This is primarily due to a significant improvement in signal-to-noise ratio, which is more noticeable for smaller torque amplitudes. Overall, motion profiles with speed offset lead to an improved correction behavior for all approaches. This is due to additional stick-slip effects for acceleration movements and not yet included correction of motor torques when decelerating until standstill. In combination with smaller deviations in modeled friction torque, this effect is more significant for low torque amplitudes (e.g. $A_1$-$O_1$).

The right part of figure 7 shows the results for increased acceleration and jerk limits $\dot{\varphi}_{max,2}$ and $\ddot{\varphi}_{max,2}$. This deliberately dynamically chosen parameterization serves to show limits of the respective correction approaches. In case of $A_4$ and $A_5$, the torque limit is reached when moving from or to standstill as well as when decelerating with offset $O_2$. As expected, this is no limitation for all actual value-based approachs ($V_1$, $V_2$ and $V_3$). In case of $V_{4a}$ and $V4_b$, consideration of nonlinear torque limitation during parameter identification is not provided due to the structure of the underlying system model. Consequently, significantly higher deviations occur compared to actual value-based methods. For all other motion sequences, command value-based approaches show good agreement between modeled and measured acceleration torques, regardless of the specific parameterization (individual or averaged).

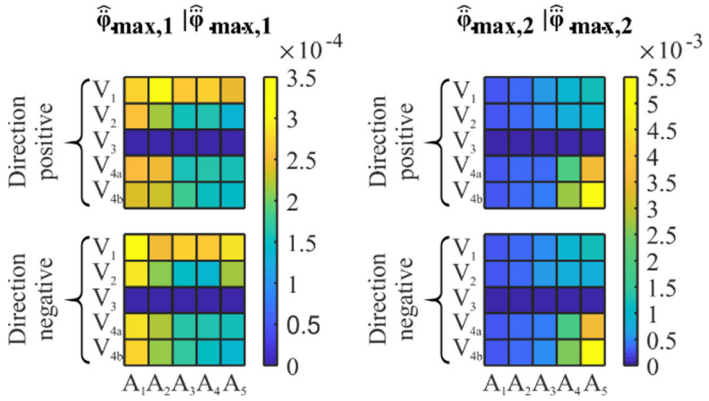


Figure 8: $A_{IAE}$ of acceleration correction approaches for direction reversal with preset (left) and increased values for acceleration and jerk limitation (right).

In addition, several experiments were conducted to evaluate the approaches in case of direction reversal. These are considered separately due to their increased requirements for acceleration correction. The axis is first accelerated to a constant velocity according to table 1. Subsequently, the speed setpoint value changes its sign. Due to higher accelerations, acceleration and torque limits are reached more frequently. Furthermore, stick-slip effects as well as additional slack in the reversal range are challenges for an exact acceleration torque estimation. All magnitudes and limitations for jerk and acceleration correspond to the values from table 1. Again, figure 8 summarizes the results based on $A_{IAE}$ over the weighting area $\gamma_a$.

The left part of figure 8 represents the remaining deviations with preset values for acceleration and jerk limits when accelerating in positive and negative direction, respectively. Regardless of the speed amplitude, it becomes clear that besides an ideal acceleration correction according to approach $V_3$, setpoint-based methods $V_{4a}$ and $V_{4b}$ again achieve highest accuracy. This also applies in case of acceleration-limited motion profile, as it occurs for $A_3$ to $A_5$. A parameterization based on averaged setting values leads to better or equivalent results compared to an individual setting.

However, a more dynamic setting for acceleration and jerk limits ($\dot{\ddot{\varphi}}_{max,2}$ and $\ddot{\ddot{\varphi}}_{max,2}$) shows that command value-based approaches cannot achieve appropriate estimation results, especially for higher magnitudes ($A_5$). Once more, the main reason is that the torque limit is reached. Furthermore, it should be noted that the detection of the weighting area is no longer fully successful due to high overshoot in actual torque value. Regarding actual value-based methods $V_1$ and $V_2$, an increased estimation quality in case of inverse filtering is confirmed again. This can be observed independent of applied motion profile or parameterized limits for acceleration or jerk.

## 4 DISCUSSION

Overall, approach $V_3$ leads to an ideal correction of acceleration torques for all investigated positioning sequences. Hence, it represents the preferred solution. However, if external load torques act during acceleration phases (e.g. in event of collision), a command value-based approach ($V_4$) offers a valuable option. Parameterization based on several averaged parameter sets does not compulsorily lead to reduced accuracy compared to a speed-related setting. Hence, this approach is much more robust than the method presented in (Kaever, 2004), which requires an additional variation of gain factors depending on actual motor speed. Merely in case of dynamic motion profiles with reversal of direction or while reaching torque limit, a command value-based approach is not recommended. If no position command signal is available, approach $V_2$ achieves a sufficient acceleration correction in combination with parallel weighting of acceleration phases. Although the commissioning procedure is more complex compared to approach $V_1$, $V_2$ leads to a significantly better approximation for all examined motion sequences.

## 5 CONCLUSION

Within the scope of the paper, four approaches for a correction of acceleration phases in motor torque signal of electromechanical axes were developed and experimentally investigated. It has been shown that

an increased modeling depth equally leads to an improvement of the estimation quality. In addition, the described weighting function enables a detection of acceleration and braking phases. This allows an ideal correction by subtracting the actual motor torque in the detected range. Main advantage of the presented command value-based approach is asignificantly lower noise of the artificial acceleration signal. Furthermore, the approach operates independently of any additional external loads that may act during acceleration phases (e.g. process forces). By comparing all variants for a wide range of acceleration and braking situations using extensive experimental tests, a performance evaluation of all approaches is carried out. Hence, the results of the paper may be used to select suitable approaches for specific application scenarios.

Future work should examine the influence of superimposed external load torques on the acceleration correction. Additionally, an adequate reconstruction of external load forces requires the estimation of further operation-related effects in the motor torque signal. Besides already corrected frictional torques, periodic disturbances caused by motor poles and notches should be compensated. Furthermore, conducted experiments have shown that motor torque does not drop to zero in case of axis standstill. Main cause are effects in the current control loop. However, these sections in the motor torque signal must be detected and corrected. Eventually, an inverse transfer function between the initiation point of an external load torque at the end of the mechanical chain and the measured motor torque must be modeled. Therefore, it should be examined to what extent the discrete method presented needs to be adapted.

## ACKNOWLEDGEMENTS

Supported by:
ZIM Zentrales Innovationsprogramm Mittelstand
Federal Ministry for Economic Affairs and Climate Action
on the basis of a decision by the German Bundestag

Funded by the Federal German Ministry for Economic Affairs and Climate Action.

## REFERENCES

Quellmalz, J. et. al. (2016). Performance Index for Servo Drives under PI Speed Control. In*: Solid State Phenomena* 251, pp. 152 – 157.

Schöberlein, C. et. al. (2022a). Sensorless Condition Monitoring of Feed Axis Components in Production Systems by Applying Prony Analysis. In: *Proceedings of the 19th International Conference on Informatics in Control, Automation and Robotics - ICINCO*, pp. 214 – 221.

Kaever, M. (2004). Steuerungsintegrierte Fertigungsprozeßüberwachung bei spanender Bearbeitung. Dissertation, Rheinisch-Westfälische Technische Hochschule Aachen.

Aslan, D., Altintas, Y. (2018). Prediction of Cutting Forces in Five-Axis Milling Using Feed Drive Current Measurements. In: *IEEE/ASME Transactions on Mechatronics* 23(2), 2, pp. 833 – 844.

Aslan, D. (2019). Integration of Virtual and On-line Machining Process Control and Monitoring using CNC Drive Measurements. Dissertation, University of British Columbia.

Yamato, S. et. al. (2019). Enhancement of Sensor-less Cutting Force Estimation by Tuning of Observer Parameters from Cutting Test. In: *Procedia Manufacturing 41*, pp. 272 – 279

Yoneka et. al. (2012). Disturbance Observer–Based In-process Detection and Sup-pression of Chatter Vibration. In: *Procedia CIRP 1*, pp. 44 – 49

Sugiyama et. al. (2017). Development of sensorless chatter detection method in ball screw drive system applying mode decoupling. In: *Proceed-ings IECON 2017 - 43rd Annual Conference of the IEEE Industrial Electronics Society*, pp. 3185 – 3190

Yamato et. al. (2021). Development of Automatic Chatter Suppression System in Parallel Milling by Real-Time Spindle Speed Control with Observer-Based Chatter Monitoring. In: *International Journal of Precision Engineering and Manufacturing 22(2)*, pp. 227 – 240

Rehse, M. (1999). Flexible Prozessüberwachung bei der Bohr- und Fräsbear-beitung in einer Autonomen Produktionszelle. Dissertation, Rheinisch-Westfälische Technische Universität Aachen

Rudolf, T. (2014). Adaptierbare Parametrierung von Diagnosesystemen durch Verwendung digitaler Antriebssignale in der Prozessüberwachung. Dissertation, Rheinisch-Westfälische Technische Hochschule Aachen.

Schöberlein, C. et. al. (2022c). Modeling and Identification of Friction and Weight Forces on Linear Feed Axes as Part of a Disturbance Observer. In: *International Journal of Mechanical Engineering and Robotics Research 11(4),* pp. 198 – 206.

Isshiki, K. et. al. (2021). Enhancement of Accuracy in Sensorless Cutting-Force Estimation by Mutual Compensation of Multi-integrated Cutting-Force Observers. In: *Proceedings of the Machining Innovations Conference for Aerospace Industry (MIC)*, pp. 33 – 40.

Hellmich, A. et. al. (2011). Non-Invasive Parameter Identification by using the Least Squares Method. In: *The Archive of Mechanical Engineering 8 (2)*, pp. 185 – 194.

Hofmann, S. et. al. (2010). Identification of Parametric Models for Commissioning Servo Drives. In. *Brezina, T., Jablonski, R. (eds) Recent Advances in Mechatronics.* Springer, Berlin, Heidelberg.

Hipp, K. et. al. (2017): Simulation based optimization for controller parameterization of machine tool axes – advanced application. In: *Journal of Machine Engineering* 17(1), pp. 57 – 68.

Schöberlein, C. et. al. (2022b). Identification and Discrete Inversion of Multi-Mass Systems as Part of a Disturbance Observer. In: *Proceedings of the 2nd Winter IFSA Conference on Automation, Robotics and Communications for Industry 4.0*, pp. 13 – 18

Siemens AG (2012): Servo Drive Optimization Guide SINAMICS S120 / SIMOTION D. Technical Specification.

Nelder, J., Mead, R. (1965). A Simplex Method for Function Minimization. In: *The Computer Journal Advance* 7, pp. 308 – 313.

Schröder, Th. (2007). Entwicklung und Evaluation von Algorithmen zur zeitoptimierten Bewegungszerlegung bei kinematisch redundanten Werkzeugmaschinen. Dissertation, Technische Universität Chemnitz.

Graf, U. (2012). Applied Laplace Transforms and Z-Transforms for Scientists and Engineers: A Computational Approach Using a Mathematica Package. Switzerland, *Birkhäuser Basel*.

Schilling, R. J., Harris, S. L. (2016). Digital Signal Processing Using MATLAB. *USA, Cengage Learning*.

Groß, H.; Hamann, J.; Wiegärtner, G. (2006). Technik elektrischer Vorschubantriebe in der Fertigungs- und Automatisierungstechnik. Mechanische Komponenten, Servomotoren, Messergebnisse. Erlangen: Publicis Corporate Publishing.

Brand, C. (2002). Neuronale Identifikation von Totzeiten. Dissertation, Technische Universität München.